Sādhanā Vol. 40, Part 3, May 2015, pp. 851–861. © Indian Academy of Sciences

Effect of Hartmann layer resolution for MHD flow in a straight, conducting duct at high Hartmann numbers

SHARANYA SUBRAMANIAN[1,*], P K SWAIN[2], A V DESHPANDE[1] and P SATYAMURTHY[2]

[1]Mechanical Engineering Department, Veermata Jijabai Technological Institute, Mumbai 400 019, Maharashtra, India
[2]ADS Target Development Section, Bhabha Atomic Research Centre, Mumbai 400 085, Maharashtra, India
e-mail: 17.sharanya@gmail.com

MS received 30 July 2014; revised 6 January 2015; accepted 6 February 2015

Abstract. Conventionally, obtaining a converged solution for a MagnetoHydro-Dynamic problem entails a highly resolved Hartmann boundary layer, leading to excessive time and computational requirements. For high Hartmann number flows through electrically conducting channels, majority of the current loops close through the walls and the Hartmann layer contributes only a small fraction of the global current path. Hence, the effect on flow parameters due to coarsening the mesh of the Hartmann Layer was investigated using the ANSYS FLUENT code. Numerical simulations have been carried out in square and rectangular ducts with wall conductance ratio of 0.156 and 0.078 respectively. Magnetic field was varied from 1T to 4T to obtain solution for Hartmann numbers $\left(Ha = Ba\sqrt{\sigma/\mu}\right)$ in the range of 260–1040 for the square duct, and 520–2080 for the rectangular duct. B, a, μ, and σ are the strength of applied magnetic field, characteristic length of the channel, dynamic viscosity and electrical conductivity of the fluid respectively. The errors in estimating core and side layer peak velocity and fully developed pressure gradient were found to be low even for a grid system having 46% coarser grid than a well-resolved system. The analysis indicated that for high Hartmann number flows through thick, conducting ducts, coarsening the mesh in the Hartmann boundary layer reduced computational time, not compromising on the solution accuracy and appears to be a promising option for complex geometry MHD simulation.

Keywords. Magnetohydrodynamics; Hartmann number; test blanket module.

1. Introduction

Magnetohydrodynamics studies the flow of electrically conducting, non-magnetic fluids subjected to an external magnetic field (Muller & Buhler 2001). The relative motion of such a fluid

*For correspondence

through a channel, in the presence of an applied magnetic field sets up a transverse current, which in turn interacts with the external magnetic field to produce electromagnetic (EM) body forces (Davidson 2001). The EM body forces significantly modify the velocity and pressure distribution, creating the characteristic M-shaped velocity profile across the Side Walls (parallel to the magnetic field) and a flattened velocity profile across the Hartmann Walls (perpendicular to the magnetic field) (Hunt 1965) Although analytical solutions are available for fully developed flow with specific boundary walls (Hunt 1965), no exact solutions except models based on variational methods (Sidorenko & Shishko 1991) exist, even for a simple case of MHD flow in single duct with electrically conducting walls. Even though numerical simulations have been carried out in conducting channels at high Hartmann number with modified thin wall conditions by including Hartmann layer (thickness ∼a/Ha) (Muller & Buhler 2001), no quantitative assessment of the effect of the unresolved Hartmann layer on various flow parameters in conducting channels of different aspect ratios and hence different wall conductance ratios have been undertaken.

For realistically computing the flow field, the Hartmann and Side boundary layers- through which the induced current paths close, need to be well resolved. For instance, the MHD flow through the Test Blanket Modules (TBM) of International Thermo-nuclear Experimental Reactor (ITER) (Paritosh Chaudhuri *et al* 2012) consists of parallel/anti-parallel electrically coupled channel flow, multiple L/U bends, etc. The Hartmann number is very high (10^3–10^4) and hence, very thin Hartmann layers (thickness ∼10 μm) are formed. 3D numerical simulation of MHD flow in the entire geometry with a properly resolved Hartmann layer requires large computation time due to large grids (few million volume elements) and results in extremely slow convergence, further leading to very large computation time (many weeks to months for one set of flow rate). Thus, arriving at the optimum TBM design necessitates long simulation durations.

This work is primarily to demonstrate that computational time can be reduced by not resolving the Hartmann layer with tolerable error associated with other flow parameters. We attempt to understand the effect of coarsening and not resolving the Hartmann boundary layer thickness, $\delta_{Ha} \sim a/Ha$ on the overall solution, for channels with conducting walls like the present TBM design and thereby, establish the benchmark for code performance in a simple geometry. Square and rectangle cross-sections are studied and an FVM solution is employed using ANSYS FLUENT (2010). Liquid Metal Lead–Lithium (Pb–Li) is used as a Tritium breeder as well as a coolant in the TBM, and is thus taken as the working fluid for the present analysis. Hartmann Number for the flow has been varied from 260 to 1040 for the square duct and from 520 to 2080 for the rectangular duct by changing the magnetic field from 1T to 4T. The major purpose of this numerical analysis is to verify the accuracy of the code (essentially bench marking) so that the same code can be used in designing the TBM which consists of multi-channel flows with walls of unequal conductance.

2. Governing equations

MHD flows are described by coupling the equations governing fluid flow with Maxwell's equations of electrodynamics. The resulting, steady state, incompressible MHD equations are (Hunt 1965)

$$(\vec{\nabla} \bullet \vec{U}) = 0 \qquad \text{(Continuity equation)} \qquad (1)$$

$$(\vec{\nabla} \bullet \vec{J}) = 0 \qquad \text{(Current conservation)} \qquad (2)$$

$$\vec{J} = -\sigma(-\vec{\nabla}\phi + \vec{U} \times \vec{B}) \qquad \text{(Ohm's law)} \qquad (3)$$

$$(\vec{U} \bullet \vec{\nabla})\vec{U} = -\frac{\vec{\nabla} P}{\rho} + \nu \nabla^2 \vec{U} + \frac{\vec{J} \times \vec{B}}{\rho} \qquad \text{(Momentum equation)} \tag{4}$$

ρ, $\vec{U}$, ν, P, $\vec{J}$, σ, $\vec{B}$, and ϕ are density,velocity, kinematic viscosity, pressure, current density, electrical conductivity, applied magnetic field, and electric potential respectively.

3. Solution methodology

3.1 *Geometry description*

A square and a rectangle duct having a 25 × 25 mm and 25 × 50 mm cross-section, and length of 500 mm have been analyzed. Figure 1 shows the rectangular cross-section geometry. The wall thickness (t_w) was 1.5 mm and the field is applied along the Y-Axis. The flow of Pb–Li along the channel occurs along the Z-Axis.

3.2 *Grid generation*

For both geometries, three grid systems – Grid 1, Grid 2, Grid 3 – were designed, having 3, 1 and no points in the Hartmann boundary layer respectively at the highest magnetic field of 4T. For all systems, the Side Wall Boundary Layer thickness, ($\sim a/\sqrt{Ha}$) was resolved with 9 points at 4T field to capture the Side Layer velocity peaks. A fourth system, Grid 4, was created for both geometries, having no grid point in the Hartmann boundary layer at 1T. As the Hartmann Layer thickness goes on decreasing with field, this system provided a completely unresolved Hartmann layer at all fields higher than 1T.

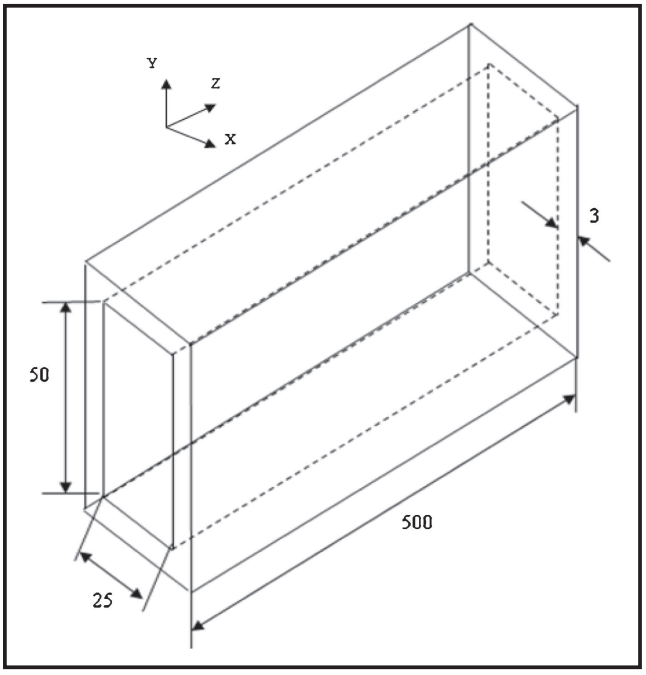

Figure 1. Rectangular geometry.

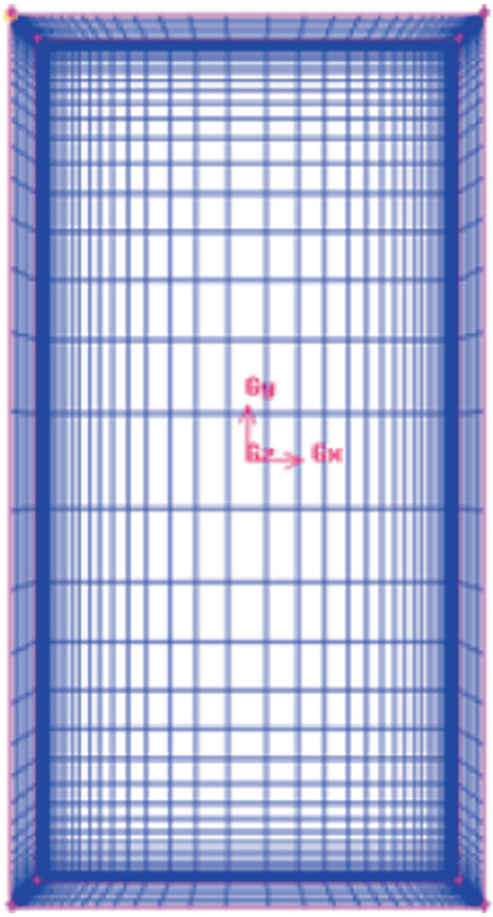

Figure 2. Rectangle geometry meshed cross-sectional.

A structured, non-uniform mesh – coarse in the core region of the flow and progressively finer towards the walls – was employed (figure 2). Meshing along the channel length was kept uniform, using a total of 70 grid points. The coarseness of the grid systems with respect to Grid 1 is summarized in table 1.

3.3 *Details of flow simulation*

The Magnetic Induction and the Electric Potential method are used to solve MHD equations. The former considers the effect of the magnetic field set up by the induced current. Here, the

Table 1. Meshing details.

Geometry	Square				Rectangle			
Grid	Grid 1	Grid 2	Grid 3	Grid 4	Grid 1	Grid 2	Grid 3	Grid 4
No. of cells	336980	285390	257250	177520	369810	318220	290080	196280
% Coarseness with respect to Grid 1	–	15.31	23.66	47.32	–	13.95	21.56	46.92

effect of induced field was neglected as the Magnetic Reynolds Number, $R_m\ (= \mu_o \sigma w a) << 1$. So the Electric Potential Method was used. Using Eq. (2) and Eq. (3), a Poisson equation for electric potential Eq. (5) is formed and solved within the flow field.

$$\nabla^2 \phi = \vec{\nabla} \bullet \left(\vec{U} \times \vec{B}\right) \tag{5}$$

For the geometries under study, since $Ha/\mathrm{Re} >> 1/300$, the laminar model was chosen for the numerical solution. A pressure-based solver was employed and the *SIMPLE* algorithm (Patankar Suhas 2011) provided Pressure–Velocity Coupling. *Second Order Upwind* was used as the discretization scheme for Electrical Potential and Momentum.

3.4 *Boundary conditions*

The inlet velocity for all cases was 0.01 m/s and was specified via a *Velocity Inlet* boundary condition and a *Pressure Outlet* boundary condition was used to set the channel outlet gauge pressure to 0 Atm. At all the inner wall surfaces, a *No-slip boundary condition* was applied and these walls were treated as coupled walls to ensure continuity of the normal component (to the walls) of current density ($J_\mathrm{n} = J_\mathrm{nw}$) and that of electric potential ($\phi = \phi_\mathrm{w}$). The outer surfaces of the wall were modeled as insulating surfaces to ensure that no electric current passes through these boundaries.

4. Results and discussions

The channels were considered to be of Stainless Steel having electrical conductivity $\sigma_w 1.01 \times 10^6$ S/m. The density of Pb–Li was taken as 9776.9 kg/m^3, its electrical conductivity 7.7616×10^5 S/m. Its dynamic viscosity and magnetic permeability were taken as 0.0018 Pa.s and 1.257×10^{-6} H.m^{-1} respectively. The wall conductance ratio, $c = \sigma_w t_w / \sigma a$ is kept constant for the square and rectangular channel at 0.156 and 0.078 respectively. The results of the numerical simulation are discussed in the subsequent sub-sections where comparisons are made between grid systems to determine effect of coarsening, and with existing analytical and numerical schemes for model validation. For ease of tabulation and discussion, magnetic field values are mentioned instead of the corresponding Hartmann Number.

4.1 *Induced current comparison*

Tables 2 and 3 compare the currents in Hartmann layer, core and walls for fully developed flow, for both the geometries and the overall current conservation for each grid system is also tabulated. At every magnetic field, the core current density, the core current and the wall current for the four grid systems agree well with each other and their variation with respect to Grid 1 does not exceed 1.5% for both geometries. Since Grid 4 for both geometries has no points in the Hartmann layer even at 1T, no value was obtained for Hartmann layer current.

At 1T, the ratio of currents in Hartmann Layer to the Hartmann wall is less than 2% for Grids 1, 2, 3 of both the geometries (tables 2 and 3). As the magnetic field is increased, the Hartmann layer becomes thinner and offers higher resistance to the global current path. This causes most of the current loops to close through the Hartmann walls instead of the boundary layer, reducing the Hartmann layer current. In fact, the ratio of current in Hartmann layer to the Hartmann wall is less than 0.5% even for the finest grid system (Grid 1) at 4T.

Table 2. Variation of currents for square geometry with magnetic field (c = 0.156).

Property	Magnetic field* (T)	Grid 1	Grid 2	Grid 3	Grid 4
Core current density (A/m^2) at centre of channel	1	−883.59	−883.16	−882.81	−876.16
Core current (A/m)		−21.83	−21.81	−21.8	−21.52
Wall current (A/m)		21.48	21.49	21.49	21.51
Current in Hartmann layer (A/m)		0.36	0.36	0.35	0
Hartmann layer current to wall current ratio		0.0168	0.0169	0.0162	0
Current conservation percentage		0.933	1.094	1.342	1.774
Core current density (A/m^2) at centre of channel	4	−3296.31	−3296.71	−3297.2	−3285.31
Core current (A/m)		−82.15	−82.12	−82.09	−82.02
Wall current (A/m)		82.05	82.02	81.98	82.03
Current in Hartmann layer (A/m)		0.33	0.3	0.15	0
Hartmann layer current to wall current ratio		0.0041	0.0037	0.0019	0
Current conservation percentage		1.114	2.115	3.038	0.002

*1T and 4T for square geometry corresponds to Ha of 260 and 1040 respectively.

For a given magnetic field, the number of grid points in the Hartmann layer reduces from Grid 1 to Grid 4, resulting in a lower estimation of Hartmann layer currents for both the geometries. The deviations of Hartmann layer current for Grid 2, 3, 4 with respect to Grid 1 for 1T and 4T fields are documented in table 4.

Although the Hartmann layer current is totally neglected in Grid 4 and high deviations are observed in Grid 2 and 3, overall current balance for the system is maintained (tables 2 and 3). This is because the Hartmann current accounts for not more than ∼2% of the total current. Thus, coarsening of the Hartmann layer does not affect the currents developed in the system.

Table 3. Variation of currents for rectangle geometry with magnetic field (c = 0.0.078).

Property	Magnetic field* (T)	Grid 1	Grid 2	Grid 3	Grid 4
Core current density (A/m^2) at centre of channel	1	−414.8	−414.85	−414.96	−411.87
Core current (A/m)		−20.59	−20.59	−20.59	−20.35
Wall current (A/m)		20.24	20.24	20.23	20.29
Current in Hartmann layer (A/m)		0.40	0.4	0.39	0
Hartmann layer current to wall current ratio		0.0198	0.0197	0.0194	0
Current conservation percentage		0.78	0.99	1.30	1.20
Core current density (A/m^2) at centre of channel	4	−1499.15	−1499.02	−1497.79	−1485.27
Core current (A/m)		−74.81	−74.80	−74.72	−74.19
Wall current (A/m)		74.54	74.54	74.57	74.95
Current in Hartmann layer (A/m)		0.37	0.31	0.19	0
Hartmann layer current to wall current ratio		0.005	0.0042	0.0025	0
Current conservation percentage		1.22	2.03	2.70	1.03

*1T and 4T for Rectangle Geometry corresponds to Ha of 520 and 2080 respectively.

Table 4. Percentage deviation of Hartmann layer current.

Quantity	Magnetic field (T)	Percentage error with respect to Grid 1					
		Square (c = 0.156)			Rectangle (c = 0.078)		
		Grid 2	Grid 3	Grid 4	Grid 2	Grid 3	Grid 4
Hartmann layer current	1	0.66	3.66	100	0.75	2.19	100
	2	5.13	14.45	100	1.41	15.11	100
	3	11.32	44.98	100	5.20	18.31	100
	4	10.5	54.65	100	15.16	48.89	100

Table 5. Comparison of numerical and semi-analytical core current density.

Magnetic field (T)	Core current density (A/m^2)	Square (c = 0.156)		Rectangle (c = 0.078)	
		Grid 1	Grid 4	Grid 1	Grid 4
1	Numerical	−883.6	−876.16	−414.8	−411.87
	Semi-analytical	−863.16	−862.69	−409.74	−410.56
4	Numerical	−3296.31	−3285.31	−1499.15	−1485.27
	Semi-analytical	−3282.87	−3280.53	−1488.89	−1495.83

Table 6. Core velocity.

Magnetic field (T)	Core velocity (m/s) square (c = 0.156)				Core velocity (m/s) rectangle (c = 0.078)			
	Grid 1	Grid 2	Grid 3	Grid 4	Grid 1	Grid 2	Grid 3	Grid 4
1	0.00823	0.00823	0.00823	0.00823	0.00729	0.00729	0.00729	0.00730
4	0.00783	0.00783	0.00782	0.00782	0.00662	0.00662	0.00662	0.00665

Table 7. Comparison of numerical and semi-analytical core velocity.

Magnetic field (T)	Grid system	Core velocity (m/s) square (c = 0.156)			Core velocity (m/s) rectangle (c = 0.078)		
		Numerical	Semi-analytical	% Error	Numerical	Semi-analytical	% Error
1	Grid 1	0.00823	0.00820	0.44	0.00729	0.00720	1.18
	Grid 4	0.00823	0.00821	0.27	0.00730	0.00722	1.13
4	Grid 1	0.00783	0.00783	0.03	0.00662	0.00663	0.11
	Grid 4	0.00782	0.00782	0.01	0.00665	0.00667	0.20

The core current (J_{xc}) for grid systems of both geometries in a fully developed region can be estimated using the relation $J_{xc} = -\frac{c}{1+c}\sigma w_c B$, where w_c is core velocity. (Swain *et al* 2013). This comparison is shown in table 5 for the two extreme cases – Grid 1 and Grid 4 of both geometries at 1T and 4T fields. The variation in the core current obtained from FLUENT and the semi-analytical relation does not exceed 2.5%, validating the model used.

4.2 *Core velocity comparison*

Due to the strong breaking effect of the Lorentz force, the central portion of the duct experiences a constant core velocity. A comparison among the grids with regard to core velocity is summarized for 1T and 4T magnetic field in table 6. Errors are to the tune of 0.5% or lesser for both geometries. These values of core velocities are compared with the semi-analytical relation

(Swain *et al* 2013) given by $w_c = -\frac{1+c}{B}\frac{\partial \varphi_h}{\partial x}$ in table 7 for Grid 1 and Grid 4 of both geometries. $\frac{\partial \varphi_h}{\partial x}$ represents the transverse electric potential gradient at the Hartmann wall, in a fully developed flow regime.

The general trend observed is that the errors between the numerical and semi-analytical solution reduce with increase in the magnetic field. This can be attributed to the fact that at higher magnetic fields, due to reduced Hartmann layer thickness, most of the current will close through the Hartmann walls. So, the error in estimation of electric potential gradient in the Hartmann wall is less. At lower magnetic field, since Hartmann layer contribution to the global current

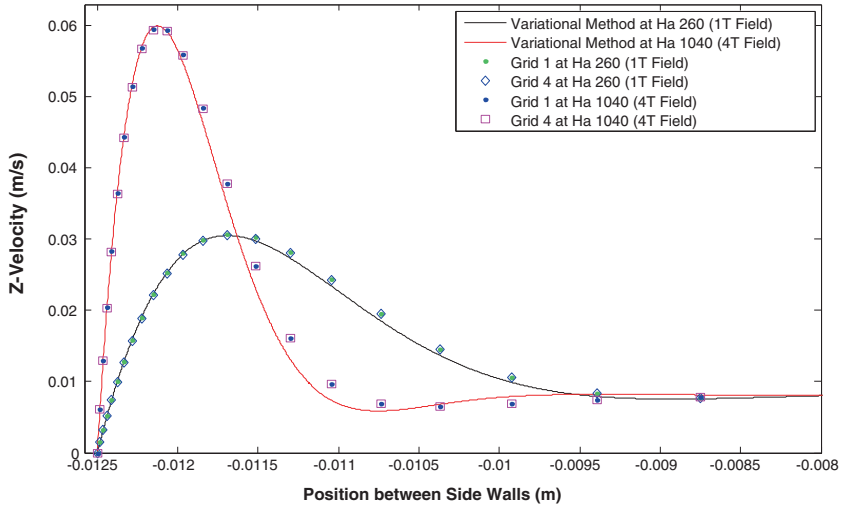

(a)

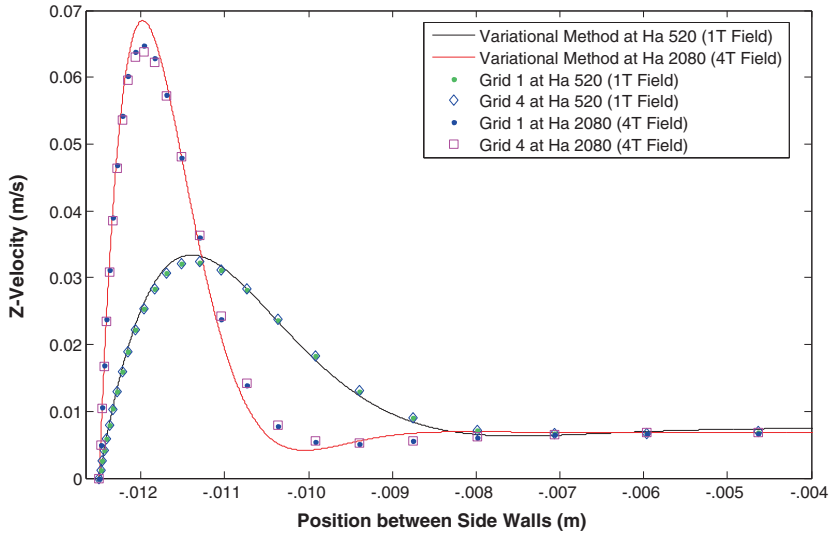

(b)

Figure 3. Z-Velocity (a) Square grid systems. (b) Rectangle grid systems.

path is considerable, neglecting this current will lead to an error in estimation of Hartmann wall potential gradient. As the core velocity is proportional to Hartmann wall potential gradient, lower potential gradient will lead to under estimation of numerical core velocity at lower magnetic fields thereby, increasing the error as shown in table 7. Variation in the grid system, however, does not give any appreciable change in the semi-analytical estimation of core velocity, for both geometries. As similar trends are observed for intermediate fields, only 1T and 4T are tabulated.

Since there is no exact analytical solution for MHD flows in a conducting channel, comparison of the fine grid system result was also carried out with existing model based on variational method approximation (Sidorenko & Shishko 1991). In this method solution is obtained for coupled velocity and induced magnetic field, expanded in terms of suitable basis function complying with the boundary conditions. The coefficients are optimized so as to minimize the residuals. The core velocities for Grid 1 of both geometries have been compared with the solution obtained from variational method and for both geometries, a maximum error of less than 4% is observed, again validating the model used in this study.

4.3 *Peak velocity comparison*

Formation of current loops leads to a parabolic distribution of electric potential along the length of the Side wall, with maximum potential difference developed at the centre. Since the current density entering the side wall is constant, the maximum potential at the centre of the side wall leads to higher electric field and hence as per Ohm's law Eq. (3), the local velocity in side layer increases. The variation in the velocity profile within the Side Layers is shown in figure 3. The comparison is done at 1T and 4T, between Grid 1, Grid 4 and a solution that is obtained from variational method. The intermediate fields have not been shown due to similarity in trends. Figure 3 shows a close agreement in the Side layer peak velocity between the fine and the coarse

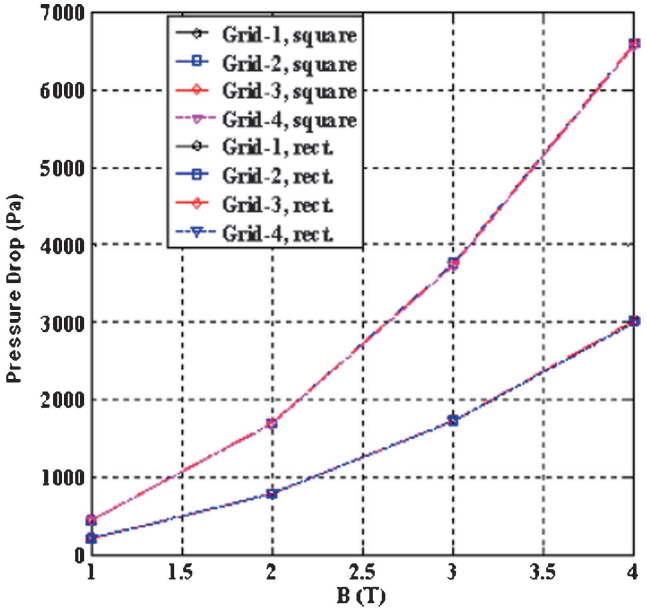

Figure 4. Variation of pressure drop with applied magnetic field for various grid systems.

grid systems. The fine grid system also matches with the analytical solution. However, higher deviations of about 5% are observed for Grid 1 of the Rectangle channel on comparison with analytical solution, indicating that Grid 1 may have to be further refined to increase accuracy.

4.4 *Pressure drop comparison*

Figure 4 shows the pressure drop developed in the flow at varying magnetic fields, for the grid systems under study. From these values, the developed flow pressure gradient was also calculated. The percentage deviations, in both the pressure drop and developed flow pressure gradient with respect to Grid 1 do not exceed 1%. The pressure drop is directly affected by the electromagnetic force that opposes the flow, which in turn depends on the current developed. As the error obtained in current estimation due to unresolved Hartmann layer is negligible, pressure distribution is not affected.

5. Conclusions

The study reveals the influence of the resolution of the Hartmann boundary layer on the flow field for a 3D MHD, steady state problem in electrically conducting, straight, rectangular ducts. The maximum error obtained in core current and wall current estimation in the ∼48% coarser square and rectangular geometry with respect to a finely resolved system is around 1.5% for square cases and around 1.2% for the rectangular geometry. For both geometries, peak and core velocities deviated by ∼1.5% and ∼0.5% respectively, with respect to the fine system. Variations in pressure drop and developed flow pressure gradient were to the tune of 1% when compared with the fine system for both geometries. Comparison with analytical model based on variational method approximation yielded a maximum error in core velocity of 4%, validating the model used in this study. It has also been established that coarsening the grid up to 50% by not resolving the Hartmann layer in a straight duct of electrically conducting walls gives acceptable results and is a promising means for reducing the computational time and resources, for complex geometry MHD simulations. For insulating walls however, all the currents will close through the Hartmann layer, and if the layer is not sufficiently resolved, realistic capturing of the flow phenomena will not be possible. Resolution of the Side layer must be adequate for a proper mapping of the local velocity peaks that are produced in them.

In summary the result of this work will facilitate 3D simulation without resolving the Hartman layers while keeping in mind the errors associated with various flow parameters. The present work also establishes the benchmarking of the code performance in a simple geometry without resolving Hartmann layers at High Hartmann number. However, the effect of coarsening the grid in Hartmann layer of electrically coupled channels consisting of multiple perpendicular bends has to be studied for generalization of this result for a general, arbitrary geometry of conducting confining walls.

References

ANSYS FLUENT 13.0 User's Guide 2010

Davidson P A 2001 *An introduction to magnetohydrodynamics*. Cambridge University Press

Hunt J C R 1965 Magnetohydrodynamic flow in rectangular ducts. *J. Fluid Mech.* 21(part 4): 577–590

Muller U and Buhler L 2001 *Magnetofluiddynamics in channels and containers*. Springer-Verlag

Paritosh Chaudhuri, Rajendra Kumar E, Sircar A, Ranjithkumar S, Chaudhari V, Danani C *et al* 2012 Status and progress of Indian LLCB test blanket systems for ITER. *Fusion Eng. Des.* 87: 1009–1013

Patankar Suhas V 2011 *Numerical heat transfer and fluid flow*. Taylor & Francis

Sidorenko S I and Shishko A Ya 1991 Variational method of calculation of MHD flows in channels with large aspect ratios and conducting walls. *Magnetohydrodynamics* 27(4): 437–445

Swain P K, Satyamurthy P, Bhattacharyay R, Patel A, Shishko A, Platacis E, Ziks A, Ivanov S and Despande A V 2013 3D MHD lead–lithium liquid metal flow analysis and experiments in a test-section of multiple rectangular bends at moderate to high Hartmann numbers. *Fusion Eng. Des.* 88: 2848–2859